Available online at www.sciencedirect.com
SCIENCE DIRECT
Biochimica et Biophysica Acta 1708 (2005) 375 – 392
BIOCHIMICA ET BIOPHYSICA ACTA
BBA
http://www.elsevier.com/locate/bba

Comparative kinetic analysis reveals that inducer-specific ion release precedes the mitochondrial permeability transition

Boris F. Krasnikov[a,b,d,*], Dmitry B. Zorov[b], Yuri N. Antonenko[b], Andrey A. Zaspa[b], Igor V. Kulikov[b], Bruce S. Kristal[a,c,d], Arthur J.L. Cooper[a,c,d], Abraham M. Brown[a,c]

[a]*Dementia Research Service, Burke Medical Research Institute, 785 Mamaroneck Avenue, White Plains, NY 10605, USA*
[b]*A. N. Belozersky Institute of Physico-Chemical Biology, Moscow State University, Moscow 119992, Russia*
[c]*Department of Biochemistry, Weill Medical College of Cornell University, New York, NY 10021, USA*
[d]*Department of Neurology and Neuroscience, Weill Medical College of Cornell University, New York, NY 10021, USA*

Received 2 March 2005; received in revised form 12 May 2005; accepted 17 May 2005
Available online 13 June 2005

Abstract

Relationships among the multiple events that precede the mitochondrial membrane permeability transition (MPT) are not yet clearly understood. A combination of newly developed instrumental and computational approaches to this problem is described. The instrumental innovation is a high-resolution digital apparatus for the simultaneous, real-time measurement of four mitochondrial parameters as indicators of the respiration rate, membrane potential, calcium ion transport, and mitochondrial swelling. A computational approach is introduced that tracks the fraction of mitochondria that has undergone pore opening. This approach allows multiple comparisons on a single time scale. The validity of the computational approach for studying complex mitochondrial phenomena was evaluated with mitochondria undergoing an MPT induced by Ca^{2+}, phenylarsine oxide or alamethicin. Selective ion leaks were observed that precede the permeability transition and that are inducer specific. These results illustrate the occurrence of inducer-specific sequential changes associated with the induction of the permeability transition. Analysis of the temporal relationship among the multiple mitochondrial parameters of isolated mitochondria should provide insights into the mechanisms underlying these responses.

Keywords: Mitochondria; Permeability transition; Multiparameter recording; Kinetic analysis; Ion leak

1. Introduction

Mitochondria perform many important cellular functions including the generation of the electrochemical proton gradient with subsequent ATP synthesis, heat production, detoxification, propagation of cell death cascade signaling, steroid and heme synthesis, amino acid metabolism, production of cellular signals, and regulation of cellular ionic homeostasis, particularly Ca^{2+} (summarized in [1]). A critical role in programmed cell death ascribed to mitochondria is attributed to the mitochondrial permeability transition (MPT) [2]. The induction of MPT results in the opening in the inner mitochondrial membrane of a non-specific pore, permeable to all solutes and small peptides with molecular masses up to 1500 Da. Such rupture of the mitochondrial membrane causes changes in a number of mitochondrial parameters. Many investigators agree with Hunter and Haworth, who suggested that the process of high amplitude swelling of mitochondria is the final phase of the MPT

Abbreviations: MPT, membrane permeability transition; $\Delta\Psi$, mitochondrial membrane potential; PhAsO, phenylarsine oxide; TPP^+, tetraphenylphosphonium; PC, personal computer; LED, light-emitting diode; PD, photodiode; ADC, analog–digital converter; DAC, digital–analog converter; BSA, bovine serum albumin; RLM, rat liver mitochondria; RCR, respiratory control ratio; CsA, cyclosporin A

* Corresponding author. Present address: Dementia Research Service, Burke Medical Research Institute, 785 Mamaroneck Avenue, White Plains, NY 10605, USA. Tel.: +1 914 597 2142; fax: +1 914 597 2757.
E-mail address: bkrasnik@burke.org (B.F. Krasnikov).

0005-2728/$ - see front matter © 2005 Elsevier B.V. All rights reserved.
doi:10.1016/j.bbabio.2005.05.009

induction [3–5]. However, the order of the mitochondrial parameter changes related to MPT induction still remains unclear.

Under in vitro experimental conditions, mitochondrial respiration is commonly monitored electrochemically using a Clark-type electrode [6]. Redistribution of the membrane-permeable cation tetraphenylphosphonium (TPP^+) can be used as an index of $\Delta\Psi$ as measured by a TPP^+-selective electrode [7,8]. Mitochondria can modulate cellular Ca^{2+} levels through highly regulated Ca^{2+} uptake and release driven by $\Delta\Psi$ [9]. Ca^{2+} ion-selective electrodes can be used to monitor the Ca^{2+} content in experimental media as a reflection of Ca^{2+} fluxes in cells or organelles [10]. In vitro, the mitochondrion behaves as an osmometer changing its ion content in parallel with the entry or exit of water (see the Discussion). Thus, $\Delta\Psi$ (a driving force for ion transport through the inner membrane) determines the distribution of osmotically active ions and water across the inner membrane and hence the mitochondrial volume. The mitochondrial volume can be monitored by light transmission changes.

Single-parameter monitoring is sufficient for many applications, but does not provide a detailed picture of mitochondrial functioning. Monitoring of several parameters can provide a more detailed description of a particular phenomenon. In addition, simultaneous monitoring of multiple parameters after the addition of a stimulus can reveal temporal links among mitochondrial changes that cannot be obtained from single-parameter recordings.

A challenge for recording simultaneous measurements is to incorporate different sensors into a single small-volume apparatus that is convenient to use and avoids interference among the different sensors. Correct analysis and integration of data from multiple channels are also critical for the development of newer models of mitochondrial function.

Previous reports described methods for the simultaneous measurements of different parameters of mitochondrial functioning in a variety of combinations (e.g., [11–23]). However, these studies lacked an important feature of the present work, namely, the comparative analysis of data made possible by digital signal acquisition and processing. The present analysis can provide additional information needed for determining the detailed mechanism of reactions in mitochondria induced by a given stimulus.

We describe here an integrated apparatus that allows real-time simultaneous measurement of mitochondrial oxygen consumption, $\Delta\Psi$, volume changes and external Ca^{2+} concentration, but is not limited to the measurement of only these parameters. The utility of this instrument was demonstrated in experiments that examined and analyzed the mitochondrial responses to three well-characterized MPT inducers: Ca^{2+}, phenylarsine oxide (PhAsO) and alamethicin.

2. Materials and methods

2.1. Chemicals and reagents

ADP, bis-fura-2, Biuret kit, BSA (fatty acid free), choline chloride, cyclosporin A, 2,4-dinitrophenylhydrazine, EDTA, EGTA, HCl, Hepes, L-homoserine, potassium dihydrophosphate (KH_2PO_4), sodium dithionite ($Na_2S_2O_4$), PhAsO, polyvinyl chloride, succinate and sucrose were obtained from Sigma (USA). Dibutylphthalate, tetraboron phosphonium, tetrahydrofuran and tetraphenyl phosphonium were from Aldrich (USA). Alamethicin was from Calbiochem (USA). $CaCl_2$ and Tris base were from Merck (Germany). Calcium-Ionophore I-Membrane A was from Fluka (Germany). All reagents used were of the highest purity available.

2.2. Isolation of mitochondria

An outbred, 6-month-old rat laboratory population, maintained at the A. N. Belozersky Institute of Physico–Chemical Biology of Moscow State University (Moscow, Russia), and 6-month old Fisher Brown Norway F_1 rats, maintained in the Burke Medical Research Institution animal facility (White Plains, NY), were used. Animals were fed ad libitum and had full access to water. Rats were sacrificed by decapitation. Rat liver mitochondria were isolated by a conventional differential centrifugation procedure [24] with modifications. A single liver was rapidly removed and placed in a small beaker with 40 ml of ice-cold isolation buffer containing 300 mM sucrose, 5 mM HEPES, 500 μM EDTA, 100 μM EGTA and 0.5% (w/v) BSA. The pH was adjusted with Tris base to 7.4. Minced and washed liver tissue was homogenized in a loose-fitting Dounce homogenizer (100 ml volume) at a tissue/buffer ratio of 1 g/8–10 ml. Mitochondria were isolated by differential centrifugation at 4 °C using a Beckman centrifuge equipped with a JA-20 rotor. The homogenate was initially centrifuged for 10 min at 1000×*g*. The pellet, which contained blood, nuclei and cell membrane fragments, was discarded. The supernatant fraction, which contained cytosol together with mitochondria, was carefully poured into a clean tube and centrifuged for 10 min at 10,000×*g*. The supernatant was discarded. The fat covering the interior of the centrifuge tube was carefully wiped clean using Kim-Wipes tissue. The pellet, which contained crude mitochondria, was resuspended in 5 ml of isolation buffer using a loose-fitting Dounce homogenizer (10-ml volume). The mitochondrial suspension was transferred to a clean tube and the volume was adjusted with isolation buffer to 40 ml. Mitochondria were sedimented by centrifugation for 10 min at 10,000×*g*. The supernatant was discarded and the interior of the centrifuge tube was wiped cleaned. The mitochondrial pellet consisted of light and dark brown layers. Five milliliters of washing buffer (300 mM sucrose, 3 mM Hepes, pH 7.4, adjusted with Tris base) was added to the pellet and the light

brown layer was dislodged by gentle agitation. The dark brown pellet was resuspended in 5 ml of washing buffer in a 10-ml Dounce homogenizer. The suspension was transferred to a clean tube and the total volume was adjusted with washing buffer to 40 ml. The mitochondria were centrifuged for 10 min at 10,000×*g*. To eliminate possible contamination by damaged mitochondria, the top surface of the pellet was washed twice with washing buffer, and the interior of the tube was wiped clean. The final pellet was weighed and resuspended in washing buffer at a pellet/buffer ratio of 600 mg to 1 ml to yield a final concentration of 40–50 mg protein/ml and stored on ice. Mitochondria isolated using this procedure and kept on ice were stable for over 8 h after isolation. The stability of the mitochondrial preparation was judged by the constancy of the ADP/O ratio (2.4±0.14 and 2.3±0.13; $n=4$) and respiratory control ratio (RCR) values (4.0±0.12 and 3.9±0.13, $n=4$) measured during the first hour and between 8 and 12 h after isolation, respectively. All procedures were carried out on ice in a cold room at 4 °C. Buffers, centrifuge tubes and homogenizers were kept in a bucket of ice. The mitochondrial protein concentration was determined by the micro Biuret method using the Sigma Protein Assay Kit.

Experiments were carried out using a specially designed chamber capable of the simultaneous real-time monitoring of oxygen uptake, $\Delta\Psi$, Ca^{2+} ion flux and swelling in mitochondrial suspensions.

2.3. Mitochondria purity control

γ-Cystathionase is a stable and active enzyme that is present in the liver cytosol at a relatively high concentration and is not present in the mitochondria [25]. Thus, γ-cystathionase activity can serve as a useful indicator of cytosolic contamination of the mitochondria [26]. In contrast, glutamate dehydrogenase (GDH) is a mitochondrial marker enzyme [27]. Activities of γ-Cystathionase and GDH were determined as end-point and continuous kinetic assays, respectively. γ-Cystathionase exhibited a linear activity in the liver samples for at least an hour (data not shown). Thus, the typical 5–30-min incubation period provided results that are indicative of initial reaction rates. The specific activities of γ-cystathionase and GDH are expressed as mU/mg (nmol/min/mg) of protein. Enzyme measurements were carried out in a microplate reader SpectraMax 340 system (Molecular Devices Corporation, Downingtown, PA) using untreated, medium binding, Corning 96-well clear flat bottom polystyrene microplates (Thomas Scientific Inc., Swedesboro, NJ).

The reaction mixture (50 μl) for the γ-cystathionase assay consisted of 20 mM L-homoserine (γ-cystathionase substrate) and 100 mM potassium phosphate buffer (pH 7.2). The reaction was started by sample addition. After a fixed time of incubation at 37 °C, the reaction was stopped by the addition of 20 μl of 5 mM 2,4-dinitrophenylhydrazine in 2 M HCl. Incubation was continued for an additional 5 min at 37 °C and 130 μl of 1 M NaOH was added. The absorbance of α-ketobutyrate 2,4-dinitrophenylhydrazone (ε 15,000 M^{-1} cm^{-1}) was recorded at 430 nm in a SpectraMax 340 spectrophotometer. The absorbance in the samples was determined within 2 min against a blank carried through the same procedure. Blanks consisted of buffer plus sample but no L-homoserine. γ-Cystathionase activity was measured in 2 μl of cytosolic and 5 μl of mitochondrial samples incubated for 5 and 30 min, accordingly, before the addition of the 2,4-dinitrophenylhydrazine. GDH activity was measured by the procedure of Park et al. [27].

2.4. Construction of the apparatus

The chamber (Fig. 1, Panel A) contains the main body (a), a temperature-controlled cuvette with electrodes and top stopper (b), and electronic modules (c), which provide output signals to a personal computer (PC). Input from the PC controls a magnetic stirrer (d) located below the cuvette, which allows the contents to be stirred using a Teflon-coated stirring bar. The main body of the apparatus is made from duralumin. It contains two separate compartments: one contains electronic modules (i) and another contains the temperature-controlled cuvette assembled with electrodes (ii). The entire apparatus is covered by a removable lid (iii). This design reduces interference to the optical sensor from ambient light and provides isolation from electrical noise. The temperature-controlled cuvette is made from polymethylmethacrylate and has surrounding water channels for the thermostabilization of the sample. The ratio of the surrounding water volume to inner sample volume of the closed cuvette is 15:1. The inner cuvette volume is 1.0 ml with the stopper inserted and 1–2 ml when the cuvette is open.

The cuvette design incorporates several distinctive features (Fig. 1, Panel B). The electrodes are arrayed horizontally around the cuvette and reagents are added through a channel in the center of the top stopper. This configuration prevents contact between the electrodes and the stirring bar or syringe needle used to inject reagents. A second distinctive feature is the hexagonal shape of the inner cuvette. The flat faces allow a flush fit between the inner cuvette surface and the electrodes. The smooth internal surfaces facilitate the washing of the cuvette and reduce the possibility of cross-contamination between experiments. A third feature is the conical shape of the electrode assembly, which provides a waterproof seal without the use of rubber O-rings. This design avoids recesses that would otherwise make the interior of the cuvette difficult to wash.

The electronic module (designed by AAZ, Fig. 1, Panel B) contains amplifiers (Amp) with digitally controlled programmable gains (DCPG) for four independent electrode inputs, a multiplexer, an analog–digital converter (ADC) and a digital–analog converter (DAC). The electronic module is connected to a PC. The Ca^{2+}-selective electrode (Ca) and TPP^{+}-selective electrode (TPP) have resistances of

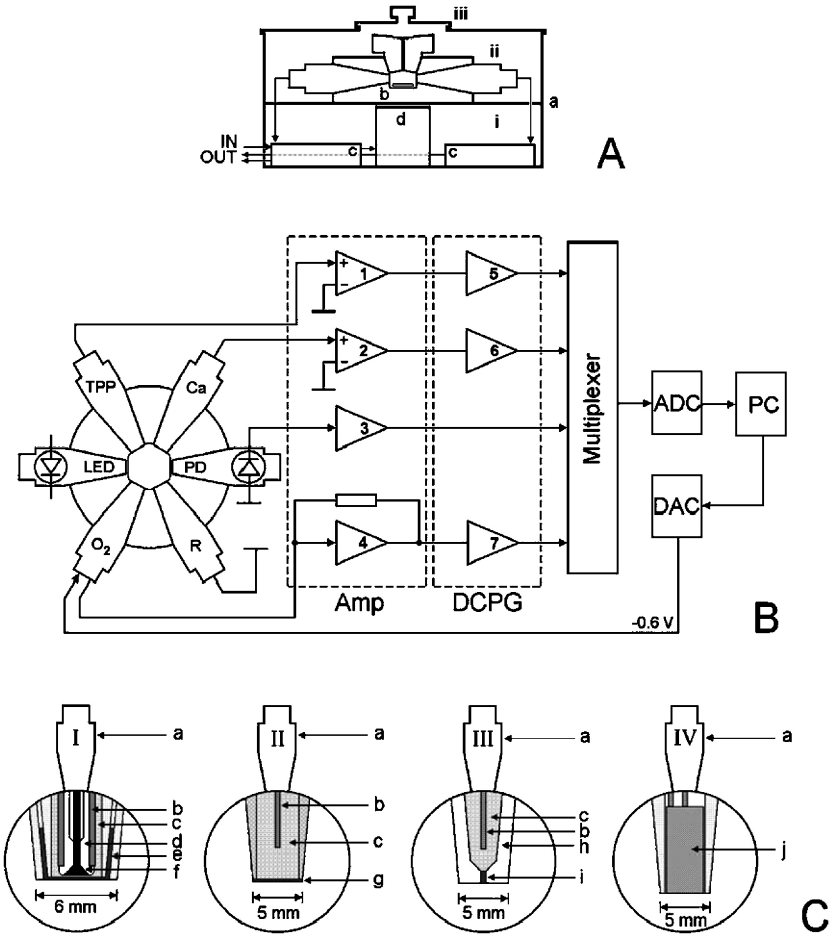

Fig. 1. Construction of the apparatus. (A) Design of the chamber: (a) main body, (b) temperature-controlled cuvette with electrodes, (c) electronic modules, (d) magnetic stirrer, (i) compartment for electronics, (ii) compartment for the temperature-controlled cuvette, (iii) removable lid. (B) Design of the temperature-controlled cuvette (median transverse section through the cuvette and electrodes) and electronic module: (O_2) Clark-type oxygen electrode, (R) reference electrode, (TPP) TPP^+-selective electrode, (Ca) Ca^{2+}-selective electrode, (LED) light-emitting diode, (PD) photodiode, (Amp) amplifiers, (DCPG) digitally controlled programmable gain stage, multiplexer, (ADC) analog–digital converter, (PC) personal computer, (DAC) digital–analog converter. (C) Design of the electrodes and sensors. (I) Clark-type oxygen electrode: (a) electrode body, (b) Ag/AgCl anode, (c) inner filling solution (3 M KCl), (d) glass module, (e) O_2-permeable membrane, (f) platinum cathode. (II) TPP^+ and Ca^{2+}-selective electrodes: (a) electrode body, (b) Ag/AgCl electrode, (c) inner filling solution (0.01 M TPPCl or 0.01 M $CaCl_2$ respectively), (g) selective membrane. (III) Reference electrode: (a) electrode body, (b) Ag/AgCl electrode, (c) inner filling solution (1 M choline chloride), (h) glass module, (i) ceramic frit. (IV) Light sensors: (a) electrode body, (j) LED or PD.

15 and 12 MΩ, respectively. The membrane potential of each electrode is measured with respect to the cuvette buffer, which is held at ground via a low-resistance (11 kΩ) reference electrode (R). The input resistance of each ion-selective electrode amplifier (1 and 2) is 10^{14} Ω, which is sufficient to prevent any contribution from the amplifier to the measured potentials. Light from the light-emitting diode (LED) is received by a hybrid photo diode (PD) that contains an integrated transimpedance amplifier. The PD output voltage, which is proportional to light intensity, is amplified by amplifier 3. A constant potential (−0.6 V) from the DAC, which is controlled by the PC, is applied to the platinum cathode of the oxygen electrode unit. The current from the oxygen electrode is converted to voltage by amplifier 4, which operates as a current–voltage converter and is then amplified by amplifier 7. Signals from amplifiers 3, 5, 6 and 7 go to the multiplexer, which sequentially connects individual amplifier outputs to the ADC. The shortest 4-channel sampling interval, which is software adjustable, is 10 ms (2.5 ms/channel). Digital data are transferred to the PC.

2.5. Construction of electrodes and sensors

The basic designs of the Clark-type, oxygen-, ion-selective and reference electrodes, and optical components are presented in Fig. 1, Panel C. The TPP^+-selective membranes for electrodes were made following the protocol previously described by Kamo and coauthors [8]. The Ca^{2+}-selective electrodes were made from commercially available membranes (Fluka # 21188). Tetrahydrofuran was used to seal membranes onto the tip of the electrode unit. The internal filling solutions for TPP^+- and Ca^{2+}-selective electrodes were: 0.01 M TPPCl and 0.01 M $CaCl_2$,

respectively. A single Ag/AgCl reference electrode with 1 M choline chloride in the internal compartment was used for both ion-selective electrodes.

2.6. Measurement of O_2 uptake by mitochondria and characteristics of the O_2 electrode

An oxygen-sensitive combination closed Clark-type electrode (Pt cathode and Ag/AgCl anode) was used for the measurement of the dissolved oxygen concentration in the experimental medium. A constant potential (−0.6 V) was applied between the cathode and anode. The electrode current, which varies linearly with the oxygen concentration (from 0 to 240 μM) in the sample solution [6], was converted to voltage, which was then sent to the ADC as described above.

Factors that limit oxygen diffusion to the platinum cathode play a crucial role in the oxygen measurement. These factors include: (i) the material used to make the oxygen-permeable membrane; (ii) its thickness; (iii) stirring of the medium; (iv) internal solution viscosity; and (v) temperature. The upper limit of the time taken by the Clark electrode to respond to an increase in oxygen tension can be determined by first allowing the electrode to locally deplete oxygen under unstirred conditions. Turning the stirrer on eliminates the area of localized oxygen depletion adjacent to the electrode surface in the unstirred buffer. The time required to initiate stirring and re-introduce oxygen to the depleted area over-estimates electrode response time. The time for 50% signal response (T_{50}) after turning on the stirrer was 0.60±0.05 s, and the time for 95% signal response (T_{95}) was 1.7±0.1 s. The electrode response time to decreased oxygen can be determined by addition of dry $Na_2S_2O_4$, which consumes dissolved oxygen. The T_{50} upon the addition of $Na_2S_2O_4$ was 0.45±0.05 s and the T_{95} was 1.5±0.1 s. The voltage dependence of the oxygen electrode on the $Na_2S_2O_4$ concentration in the buffer (O_2 concentration ranges from 0 to 240 μM) was linear and the coefficient of the regression $r^2=0.991$ (all experiments were repeated 6 times ($n=6$)).

2.7. Measurement of $\Delta\Psi$ and Ca^{2+} transport in mitochondria; TPP^+- and Ca^{2+}-selective electrode characteristics

The most important characteristic of an ion-selective electrode is the membrane potential, which is proportional to the logarithm of the chemical activity of the permeable ion in solution. The membrane potential is described by the Nernst equation:

$$E_M = \left(\frac{RT}{z_i F}\right)\log\left(\frac{a_0}{a_i}\right) \quad (1)$$

where E_M is the membrane potential; R is the universal gas constant; T is the absolute temperature in degrees Kelvin; z_i is the ion charge; F is the Faraday number; a_0 is the ion activity in the buffer; and a_i is the ion activity in the inner electrode solution.

For an ideal membrane, the dependence of voltage on the logarithm of ion concentration is described by a linear regression equation:

$$f(x) = b_0 + b_1 * x \quad (2)$$

where the coefficient b_1 reflects the Nernst potential of the membrane when $(a_0/a_i)=10$ (voltage per decade of ion concentration (slope)). In the case of monovalent ions (e.g., TPP^+) and divalent ions (e.g., Ca^{2+}), the slope b_1 for an ideal membrane is 59 mV and 29.5 mV, respectively.

TPP^+- and Ca^{2+}-selective electrode voltages are dependent on the logarithm of the ion concentration and are linear in the range 10^{-7}–10^{-4} and 10^{-7}–10^{-3} M, respectively. The slopes of the linear regression lines were 56.9 mV, $r^2=0.999$, for the TPP^+- and 24.5 mV, $r^2=0.996$, for the Ca^{2+}-selective electrodes, respectively ($n=6$).

Although we demonstrated that the electrodes could be used over a wide range of ion concentrations, the actual range encountered in typical mitochondrial experiments is much narrower. Therefore, we carried out detailed response measurements for each electrode over the relatively narrow range of ion concentrations used in typical mitochondrial experiments. Calibrations of TPP^+ and Ca^{2+} electrodes were performed by sequential additions of 0.5 μM TPPCl and 20 μM $CaCl_2$. The value of the TPP^+-selective electrode slope in the range of TPP^+ concentrations from 0.1 μM up to 2.5 μM was 56.9 mV, and the coefficient of the regression was $r^2=0.999$ ($n=6$). The slope of the regression line for the Ca^{2+}-selective electrode within the range from 5 to 100 μM was 24.8 mV and $r^2=0.999$ ($n=6$). For the TPP^+- and Ca^{2+}-selective electrodes, T_{50} was 2.9±0.6 s and 1.6±0.3 s, respectively ($n=6$). These values were not dependent on the presence of TPP^+ or Ca^{2+} initially in the buffer. In contrast, T_{95} was dependent on the prior presence of TPP^+ or Ca^{2+} in the buffer. For the first addition of TPP^+, whether 0.1 or 0.5 μM, T_{95} was 15.5±2.9 s, and for Ca^{2+}, whether 5 or 20 μM, T_{95} was 6.8±1.1 s; for the second and subsequent additions of TPP^+, T_{95} was 6.3±0.8 s and for Ca^{2+}, T_{95} was 2.7±0.3 s ($n=6$).

2.8. Detection of mitochondrial swelling

Increased transmittance in the mitochondrial suspension is correlated with mitochondrial swelling [28,29]. Measurement of transmittance was accomplished by means of the LED and PD pair at 660 nm. It was important to determine whether the PD response is linear with increasing mitochondrial concentrations. This was accomplished by comparing transmittance changes monitored by means of the LED and PD with the absorbance measurements determined at 660 nm using an Aminco DW 2000 spectrophotometer in the range of total mitochondrial protein concentration from 0.25 up to 2 mg/ml. The dependence of absorbance on the

mitochondrial concentration was linear for both an Aminco spectrophotometer ($r^2=0.997$) and the PD ($r^2=0.988$) ($n=6$). The PD response in the experimentally relevant range of 0.25–1.25 mg/ml (0.2–0.9 OD unit) was better ($r^2=0.996$) ($n=6$). The T_{50} and T_{95} PD responses to sequential mitochondrial additions in this range were 1.2 ± 0.3 and 2.3 ± 0.5 s, respectively ($n=6$). The response time of the PD after turning the LED off or on was <0.1 s ($n=6$).

2.9. Signal and data processing

Electrode and sensor output voltages were digitized using a commercially available A/D card (model L-154, L-CARD, Moscow, Russia (http://www.lcard.ru/l-154.php3)). The input voltage (−0.6 V) applied to the Clark electrode, power for the stirrer motor and the LED are provided by the onboard DAC. Software (written by IVK), which enables data import and controls the output voltages and current, operates under Windows NT. The software also enables annotation, simple data analysis, data storage and export. The data were recorded at time intervals of 0.5 s. For the mitochondrial experiments reported here, the recording time varied from about 800 up to 1400 s. Thus, the total number of points per each trace was 1600–2800. The data were imported and processed using Sigma Plot 2000.

Signal averaging was necessary because it was not possible to eliminate the low-amplitude, high-frequency electrical noise created by the amplifiers in the electrode signal. Fig. 2 presents an example demonstrating the need for signal averaging. In Panel A of this figure, an ideal sigmoidal curve generated by Sigma Plot is shown ('a' trace). The first derivative of this trace ('b') and averaged first derivative ('c') are presented in Panel B and are identical. In Panel C, low-amplitude, high-frequency noise (randomly generated by Sigma Plot) and a composite of the ideal sigmoid plot and this noise are shown as 'x' and 'a′' traces, respectively. The impact of the noise is negligible in the 'a′' trace. However, when the 'a′' trace is transformed into the first derivative (Panel D, 'b′' trace), it is difficult to recognize trends in the signal in the presence of the noise. Averaging of this noisy curve minimizes the impact of the

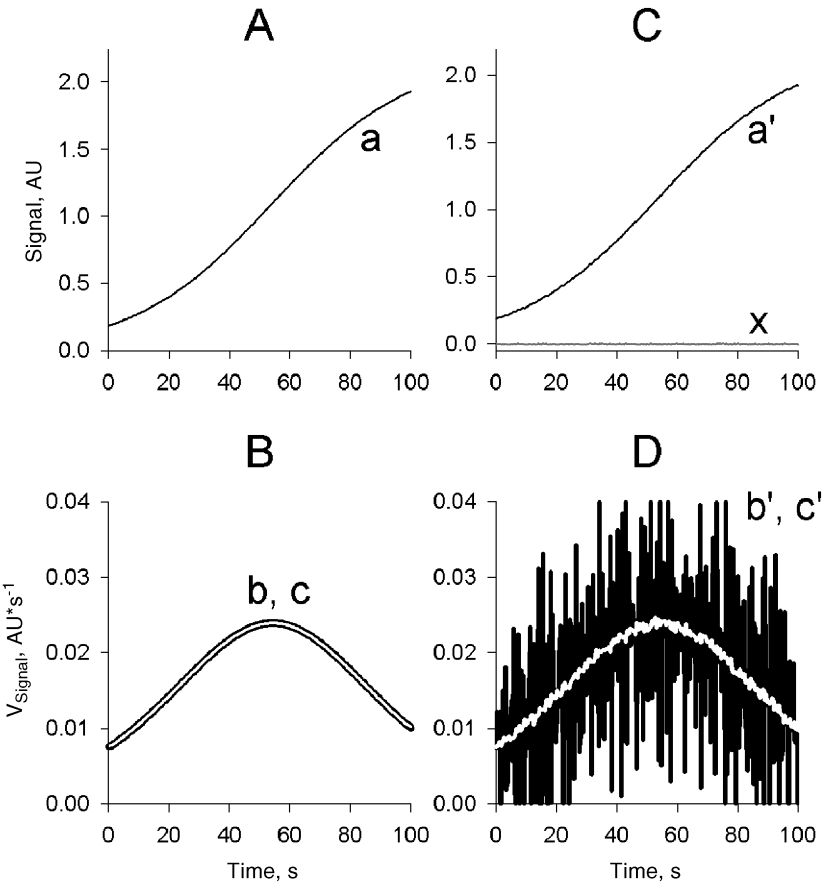

Fig. 2. Mathematical simulation of the relationship between (A) an ideal signal and (B) its first derivative, and (C) a composite of the ideal signal and noise, and (D) its first derivative. 'a' trace—ideal sigmoid (generated by Sigma Plot), 'b' trace—first derivative of the 'a' trace, and 'c' trace—averaged 'b' trace ('b' and 'c' traces are identical); 'x' trace—noise (randomly generated by Sigma Plot), 'a′' trace—composite of the 'a' and 'x' traces, 'b′' trace—first derivative of the 'a′' trace (black noisy curve), 'c′' trace—averaged 'b′' trace (white inside curve), AU denotes arbitrary units (see section 2.9 for details and explanation).

noise and allows one to clearly delineate signal changes (Panel D, 'c′' trace—white inside curve) comparable to the derivative from the ideal sigmoid plot (Panel B, 'b' trace).

2.10. Experimental conditions

All electrode calibrations were carried out at room temperature. Electrode responses were tested in buffer containing 300 mM sucrose, 10 mM HEPES, adjusted to pH 7.4 by the addition of Tris base. Mitochondrial experiments were carried out using the same buffer supplemented with 5 mM succinate and 2.5 mM KH_2PO_4, pH 7.4. Mitochondrial protein concentrations were determined by the Biuret method; except where noted, the protein concentration used in the experiments reported here was 1 mg/ml. The concentrations of the reagents added to the mitochondria in all experiments presented here were such that the total cuvette volume (1 ml) was altered by less than 1%. All additions listed in the figure legends are final concentrations. All data are presented as the mean ± S.E., except where noted.

3. Results

3.1. Additional characteristics of the TPP^+- and Ca^{2+}-selective electrodes

The Ca^{2+}-selective electrode responds to TPP^+ added to the experimental medium (Fig. 3, Panel A). One explanation for this apparent anomaly is that TPP^+ is contaminated with Ca^{2+}. This possibility was investigated using the Ca^{2+} indicator Bis-Fura-2, which showed that the 1 mM TPP^+ stock solution contained ~1.5 mM free Ca^{2+}. The Ca^{2+} contaminant was present in the TPP^+ reagent (which contained <0.1 μM Ca^{2+}, as was determined with Bis-fura-2) and not in the water used to prepare the solution. The contaminating Ca^{2+} was sequestered by the addition of 1.5 mM EGTA to the 1 mM TPP^+ stock solution (TPP*). As shown in Fig. 3, Panel B, the addition of 2.5 μM TPP* resulted in a negligible response by the Ca^{2+}-selective electrode. In contrast, the TPP^+-selective electrode did not respond to the addition of Ca^{2+} or EGTA (Fig. 3, Panels C and D).

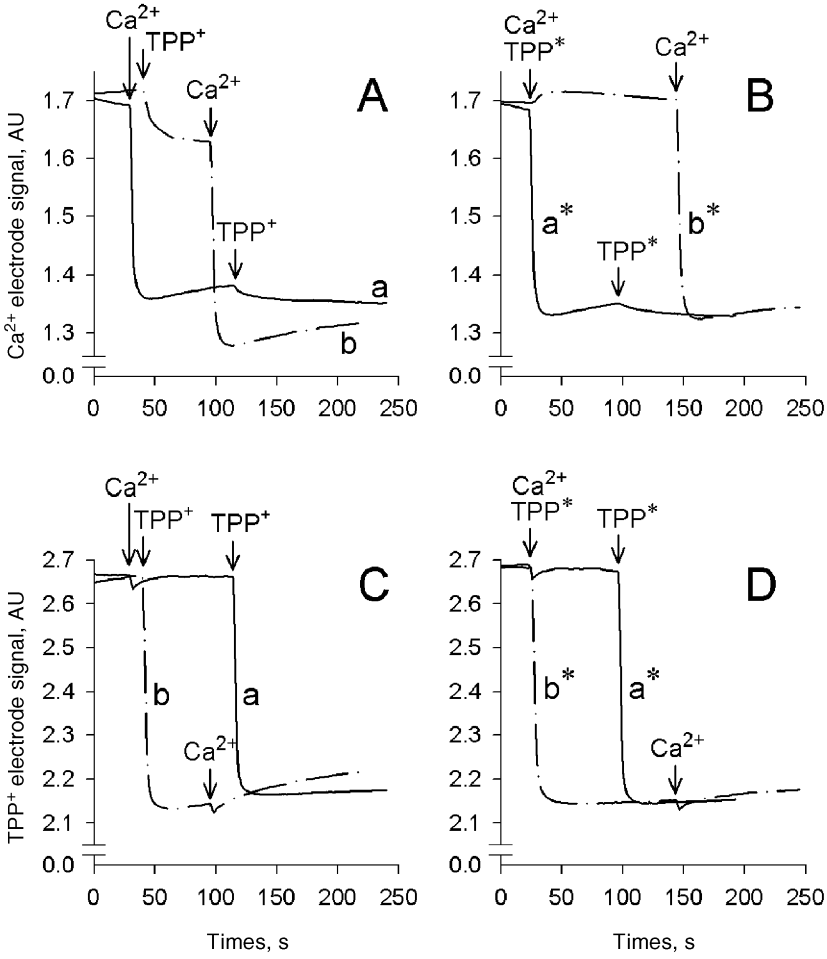

Fig. 3. Examination of (A, B) Ca^{2+}-selective and (C, D) TPP^+-selective electrodes for selectivity and interference. 'a' traces—additions of 50 μM Ca^{2+}, followed by 2.5 μM TPP^+; 'b' traces—2.5 μM TPP^+ followed by 50 μM Ca^{2+}; 'a*'—50 μM Ca^{2+}, followed by 2.5 μM TPP* (TPP*EGTA) and 'b*'—2.5 μM TPP* (TPP*EGTA), followed by 50 μM Ca^{2+}.

The absence of an electrical 'cross-talk' between the ion-selective electrodes was confirmed by comparative experiments of the mitochondrial response to Ca^{2+} load in the presence of both or only one ion-selective electrode (Fig. 4). The mitochondrial swelling response, which is indicated by increased PD signal (Fig. 4, Panel A), can be used as a reference to demonstrate that independent experiments (with different combinations of ion-selective electrodes (see sections 2.4 to 2.10 for details)) have identical kinetic characteristics. Specifically, the rate and extent of swelling in the three experiments were essentially identical (Fig. 4, Panel A). Similarly, the traces for uptake and release of Ca^{2+} from mitochondria (Panel B) and changes in $\Delta\Psi$ (Panel C) were identical when recorded in single or dual electrode experiments. The data confirmed that the TPP^+ and Ca^{2+} electrodes operate independently.

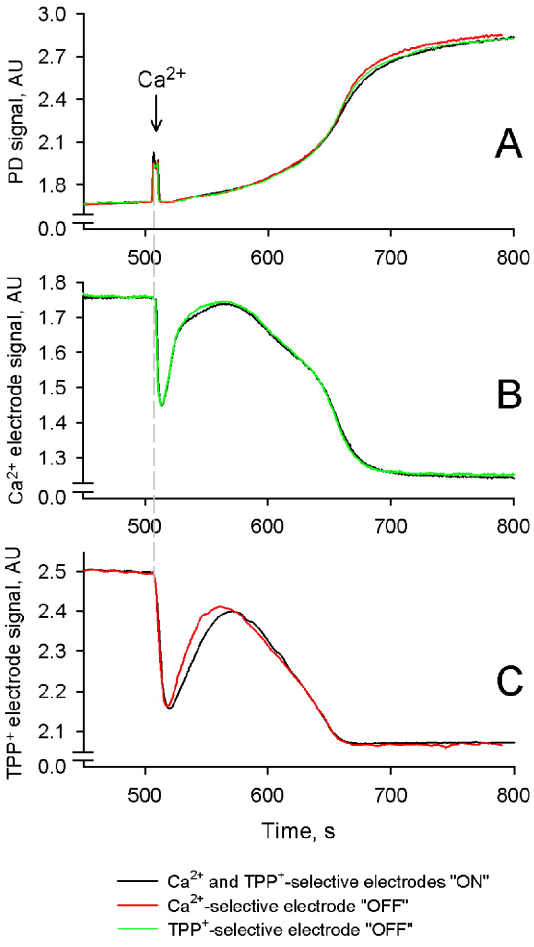

Fig. 4. Examination of Ca^{2+}-selective and TPP^+-selective electrodes for 'cross-talk'. (A) The mitochondrial swelling response serves as a reference point to confirm that in independent experiments the processes exhibit identical kinetic characteristics. (B) The Ca^{2+}-selective electrode response in the presence and absence of the TPP^+-selective electrode. (C) The TPP^+-selective electrode response in the presence and absence of the Ca^{2+}-selective electrode. MPT was induced by addition of 150 μM Ca^{2+}.

3.2. Assessment of mitochondrial purity

The specific activity of γ-cystathionase was much lower in the mitochondria compared to that in the cytosol. The values were found to be 0.63±0.01 (n=3) and 166±7 (n=3) nmol/min/mg of protein, respectively. In contrast, a very high specific activity of GDH was found in the mitochondria (3200±120 nmol/min/mg; n=4) compared to the cytosol (5.7±0.5 nmol/min/ml; n=4). Thus, the specific activity of γ-cystathionase in the mitochondria was less than 0.4% that in the cytosol. The average weight of the liver of a 6-month-old rat is ~7–8 g. The total protein in the cytosolic and mitochondrial fractions derived from this amount of liver tissue is ~1500 mg and ~40 mg of protein, respectively. Thus, one can calculate that the total activities of γ-cystathionase in the cytosol and mitochondria from an ~7-g liver are ~249,000 and 25 nmol/min, respectively. Therefore, these figures indicate that the mitochondrial fraction contained ~0.01% of the cytosolic γ-cystathionase. A similar calculation shows that >93% of the total liver GDH was present in the mitochondrial fraction. This indicates that only a small fraction of the mitochondria was damaged during isolation.

3.3. Mitochondrial experiments

Standard methods for the mitochondrial membrane permeabilization were adopted for use in the newly designed apparatus to illustrate how multiparameter analysis might be applied to gain greater insight into the mechanisms underlying this phenomenon. Ca^{2+} ions, PhAsO and alamethicin were chosen to induce permeabilization because they exert their effects through different mechanisms. Ca^{2+} induces a 'classical' MPT, resulting in transitional Ca^{2+} release and induction of osmotically driven ion fluxes [5]. PhAsO belongs to a group of MPT inducers that act through the conversion of a crucial thiol (–S–H) to a disulfide (–S–S–) [30]. Preincubation of the mitochondria with cyclosporin A (CsA) prevents the induction of MPT caused by Ca^{2+} and PhAsO [31,32]. The antibiotic alamethicin, which is a well-characterized channel former, generates pores in phospholipid and biological membranes [33,34]. Permeabilization of the mitochondrial membrane by alamethicin is not sensitive to CsA [35]. Therefore, under different experimental conditions, alamethicin serves as a control to reveal maximally possible permeabilization of the mitochondria [28,35].

Changes in the time course for oxygen uptake, Ca^{2+} flux, $\Delta\Psi$, and swelling upon the addition of 100 μM Ca^{2+}, 50 μM PhAsO or 20 μg/ml alamethicin to mitochondria from different representative experiments are shown in Fig. 5 (traces 'a'–'c', respectively). The Ca^{2+}-induced MPT is characterized by a nonlinear increase in oxygen uptake (Fig. 5, Panel A, trace 'a'), Ca^{2+} release and $\Delta\Psi$ dissipation (Panels B and C, traces 'a'), and high amplitude swelling (Panel D, trace 'a'). The PhAsO-

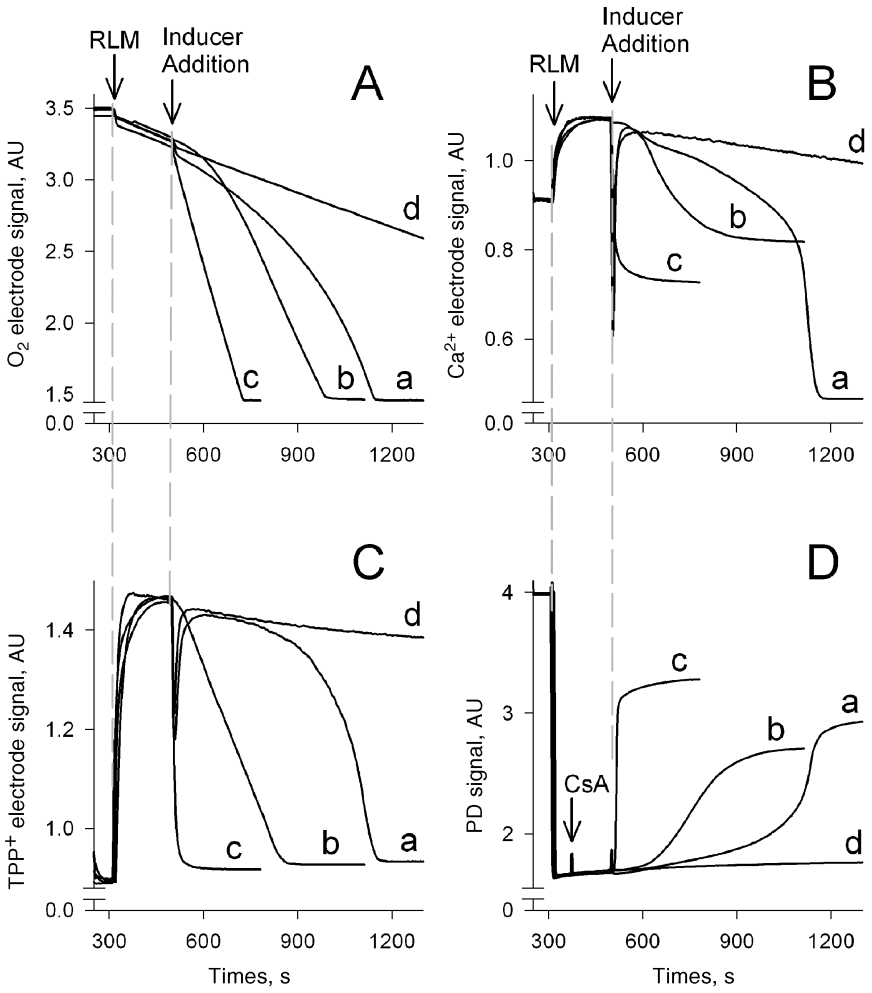

Fig. 5. Simultaneous recordings of four mitochondrial parameters representing typical mitochondrial experiments. (A) O_2 electrode signal (responds linearly to the oxygen concentration; the drop in the curve reflects a decrease of the dissolved oxygen concentration in the closed volume), (B) Ca^{2+}-selective electrode signal (the decreased Ca^{2+} electrode signal corresponds to an increase of free Ca^{2+} concentration in the buffer), (C) TPP^+-selective electrode signal [the decreased TPP^+ electrode signal correlates with an increase of free TPP^+ concentration (lower $\Delta\Psi$)], and (D) PD signal (the output of the PD is proportional to the light transmission). 'a' traces—MPT induction by 100 μM Ca^{2+}; 'b' traces—effect of 50 μM PhAsO; 'c' traces—response of mitochondria to 20 μg/ml alamethicin; 'd' traces—inhibition of Ca^{2+}-induced (100 μM) MPT by 500 nM CsA.

induced activation of MPT differs from the Ca^{2+}-induced MPT for all four-sensor readouts (Panels A–D, traces 'b'). None of these changes were observed when the mitochondria were preincubated with 500 nM CsA before the addition of Ca^{2+} (Panels A–D, traces 'd') or PhAsO (data not shown). The addition of alamethicin caused immediate changes in mitochondrial functions as reflected by a sharp linear increase of O_2 uptake, drastic release of Ca^{2+} and drop of $\Delta\Psi$, and high amplitude swelling in the mitochondria (Panels A–D, traces 'c'). CsA did not affect alamethicin-induced changes in any of the mitochondrial parameters measured (data not shown). As shown in Fig. 5, the traces of these responses are qualitatively very different in shape and magnitude for each inducer. The response to Ca^{2+} in the presence of CsA (Fig. 5, traces 'd') was included as an appropriate control for MPT. The results with Ca^{2+} plus/minus CsA also illustrates that the chamber adequately provides the appropriate responses to this well-known phenomenon. Additional controls were also carried out, including incubations with CsA and PhAsO, CsA and alamethicin, Ru360 and Ca^{2+}, and Ru360 and PhAsO. In every case, the responses were not different from the data already reported numerous times in the literature (e.g., [19,21,23,28,31,32,34,35,41,45–48]). (The data are not shown to avoid redundancy and unduly complicated figures.)

Comparison of the measured parameters for each inducer in a single plot should provide clues regarding the order of events among these parameters, leading to new insights into inducer-specific mechanisms of the MPT induction. Such analysis is complicated due to the lack of a uniform theory or mechanistic (mathematical) model that can account for multiple mitochondrial functions. The problem occurs because of the complexity of the relationships among the

various mitochondrial functions. We present a simplified model and mathematical treatment to partially address this problem (see below).

Because the electrode and PD signal outputs (except that for O_2) are logarithmic, transformation of the data to similar scales was necessary. Mathematical transformation of the electrode signals presented in Fig. 5 is shown in calibrated units in Fig. 6. This transformation clarifies the temporal changes in mitochondrial parameters. In Fig. 6, the time scale was constructed such that the zero point was at the moment of the reagent addition. A linear transformation was required to convert the oxygen electrode output into concentration units (μM). The data were then transformed to yield the rate of respiration (μMO_2 s^{-1} (first derivative) values (Fig. 6, Panel A)) to reflect the mitochondrial respiratory activity.

The inverse log transformation of the data in Panels B–D of Fig. 5 resulted in linear scales for Ca^{2+}, TPP^+ and A_{660} curves (Fig. 6, Panels B–D). The log transformation resulted in changes of both the shape and direction of the curves. The Ca^{2+} concentration (μM) was calculated from the measured Ca^{2+}-selective electrode signal (Fig. 5, Panel B) using Eq. (3), which was derived from Eqs. (1) and (2):

$$\left[Ca^{2+}\right] = 10^{\frac{\left(Ca_V^{2+} - b_0\right)}{b_1}} \tag{3}$$

where $[Ca^{2+}]$ is the concentration of $CaCl_2$ in μM and Ca_V^{2+} is the electrode potential in mV, and b_0 and b_1 are coefficients of the linear regression for the Ca^{2+}-selective electrode calibration in mV, which were derived from regular calibrations.

The TPP^+ concentration (μM) was calculated from the measured TPP^+-selective electrode signal (Fig. 5, Panel C) using Eq. (4), which was derived in a manner similar to Eq. (3):

$$\left[TPP^+\right] = 10^{\frac{\left(TPP_V^{+} - b_0\right)}{b_1}} \tag{4}$$

where $[TPP^+]$ is the concentration of TPP^+ in μM, TPP_V^+ is the actual TPP^+ electrode potential in mV, and b_0 and b_1 are coefficients of the linear regression for the TPP^+-selective electrode calibration in mV.

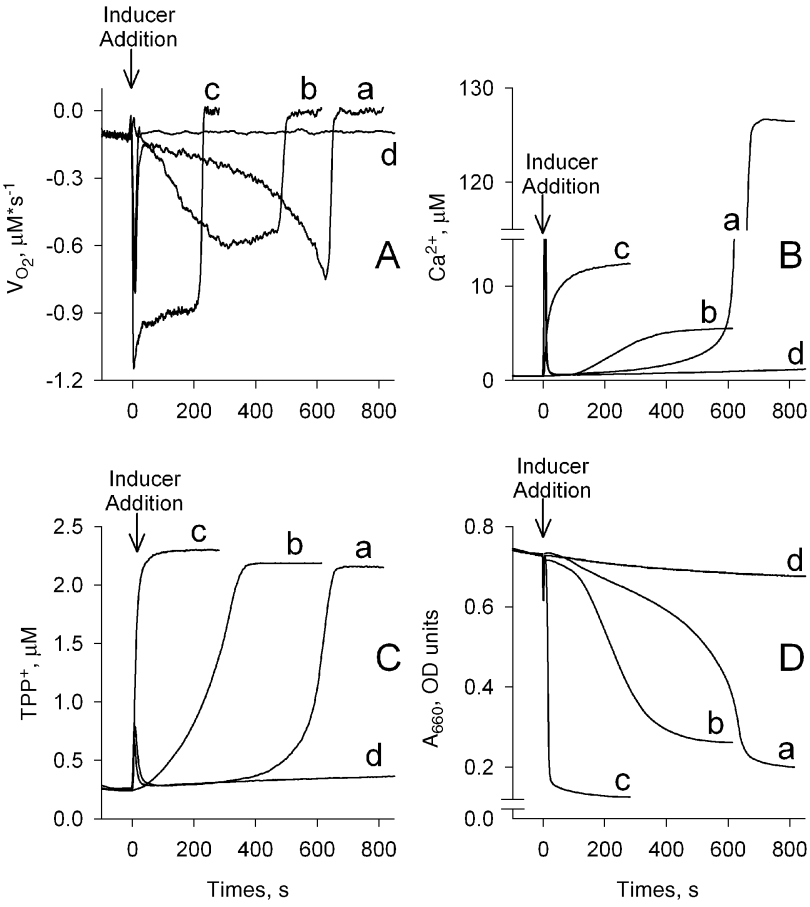

Fig. 6. Transformation of electrode signal responses from Fig. 5 into calibrated units. (A) First derivative of the oxygen electrode signal (following conversion into oxygen concentration in μM) in μM s^{-1}, (B) Ca^{2+} concentration in μM, (C) TPP^+ concentration in μM, and (D) absorbance in OD units. 'a' traces—MPT induction by 100 μM Ca^{2+}; 'b' traces—effect of 50 μM PhAsO; 'c' traces—response of mitochondria to 20 μg/ml alamethicin; 'd' traces—inhibition of Ca^{2+}-induced (100 μM) MPT by 500 nM CsA.

A negative log transformation was used to convert PD output (Fig. 5, Panel D) to absorbance (Fig. 6, Panel D). Transmittance changes, measured by the PD in mV, may be transformed into absorbance changes by using the equation:

$$Abs = -\log\left(\frac{V_d - V_i}{V_d - V_b}\right) \quad (5)$$

where Abs is absorbance, V_d is the voltage when the LED is switched off (0% transmittance), V_i is the actual voltage read out, and V_b is the voltage when the LED is switched on but no mitochondria are added to the buffer (blank) (100% transmittance).

One of the ways to compare several parameters kinetically is to present the data in a relative percent format. If the relationships among the parameters were simple (e.g., if changes occur simultaneously and equally), such an approach would be valid. Permeabilization of mitochondria by alamethicin is widely accepted as a simple model in which major mitochondrial functions change simultaneously [13,28,34]. This model is based on the fact that alamethicin "punches" holes in mitochondrial membranes eliminating the barrier between outside medium and inner mitochondrial compartments. The equilibration of ions, water, sucrose, and other small molecules may be simply ascribed to passive diffusion through these holes. Therefore, changes in the mitochondrial parameters are expected to occur simultaneously. To verify this hypothesis for each of the conditions used, the four parameters were plotted on the same scale for each of the mitochondrial permeability inducers and for the control with CsA and Ca^{2+} (Fig. 7). The maximal value of each parameter change was set as 100% (Panels A–C), except for the control with CsA, where the values for the Ca^{2+} experiment were set at 100% (Panel D). The relative change in the control (CsA and Ca^{2+}) tracings for each of the four parameters was less than 10%. Thus, the permeability of the mitochondrial membrane under such conditions was not induced. Therefore, this control was excluded from the following analysis. A commonly used method to contrast changes in multiple parameters is to compare $T_{1/2}$ values. $T_{1/2}$ values for each of the kinetics are the time points at which 50% of the maximal relative change is observed. These $T_{1/2}$ values are presented in Table 2. Note that for the control, the $T_{1/2}$

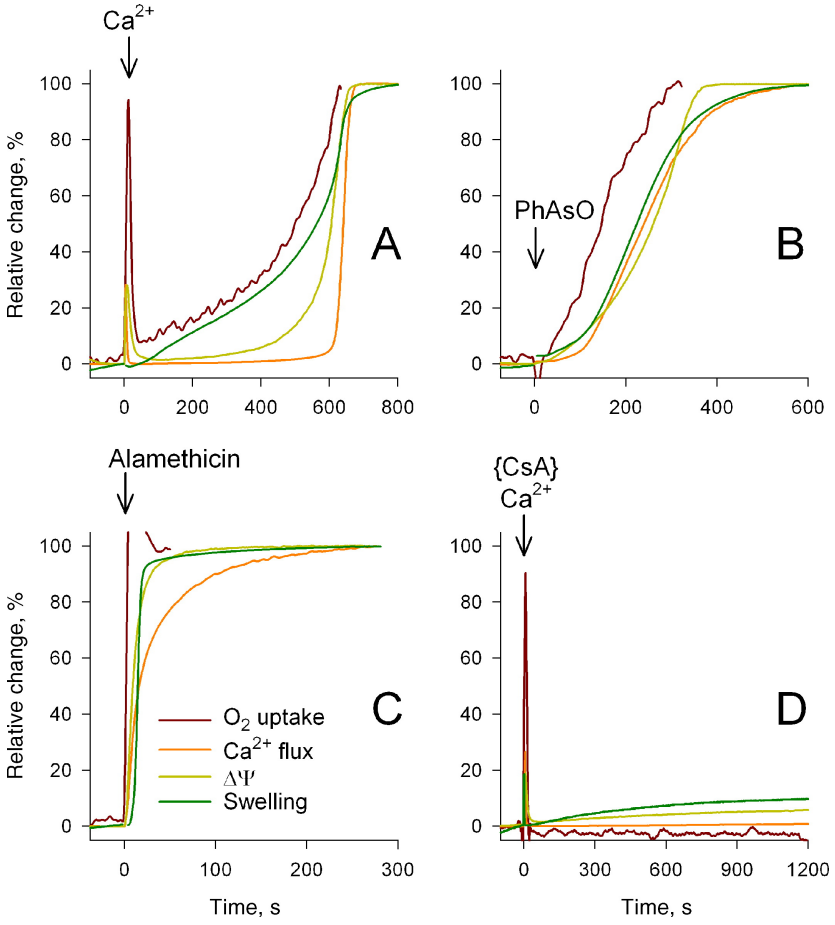

Fig. 7. Superposed and normalized traces of the relative change in parameters taken from Fig. 6. Shown are the responses of mitochondria due to MPT induction by (A) 100 μM Ca^{2+}; (B) 50 μM PhAsO; (C) 20 μg/ml alamethicin, and (D) control with 500 nM CsA and 100 μM Ca^{2+}. Note: all four traces are cut off upon reaching a relative change value of 100% (see the Results section for details and explanation).

values do not necessarily imply a monophasic process (first order kinetics).

It is clear that the difference in $T_{1/2}$ values for the measured parameters (Table 2) cannot be due to the response times of each sensor (cf. Table 1). Fig. 7 shows that the changes in mitochondrial parameters after the administration of membrane permeability inducers are not simultaneous. Even in the case of alamethicin, where the $T_{1/2}$ values varied from 1.4 to 19.3 s, such a difference might be explained either by non-simple relationships among the parameters measured or by use of an invalid approach for the analysis. A resolution of this problem is presented below.

3.4. Kinetics of mitochondrial processes assessed by population analysis

To better understand the complexity of the processes and their relationships when mitochondria are undergoing an MPT under specific conditions, the limitations of the model used must be defined. The model must first be simplified and then defined by appropriate computational approaches. The model presented in this study may be described simply as isolated mitochondria energized with succinate in isotonic (300 mosM) sucrose–phosphate–HEPES buffer. The initial state of the system may be characterized as intact/coupled mitochondria ('State 2' in the terminology introduced by Britton Chance [36]). The final state of the system may be described as swollen/uncoupled mitochondria with open pores. The transition from the initial to the final state of the system presumably includes changes in many mitochondrial parameters. As we mentioned above, the complex relationships among the mitochondrial parameters and the absence of a useful computational approach complicates the required comparisons.

Here, we present a new approach, which permits initial, semi-quantitative comparison of several parameters that characterize mitochondrial functioning. This approach is based on several assumptions, which simplify writing of equations, reflecting a transition of the mitochondrial population from the initial to the final state. The assumptions are described briefly below.

Table 1
Average sensor times (seconds) for 50% and 95% signal response (T_{50} and T_{95}) ($n=6$)

Sensor (conditions)	T_{50}	T_{95}
O_2 Clark-type electrode (stirrer turned on)	0.60±0.05	1.7±0.1
O_2 Clark-type electrode (bolus addition of $Na_2S_2O_4$)	0.45±0.05	1.5±0.1
TPP^+-selective electrode (five sequential additions of 0.5 μM TPPCl)	2.9±0.6	6.3±0.8
Ca^{2+}-selective electrode (five sequential additions of 20 μM $CaCl_2$)	1.6±0.3	2.7±0.3
LED/PD (five sequential additions of 0.25 mg/ml RLM)	1.2±0.3	2.3±0.5

Assumption 1. Opening of even one pore in a single mitochondrion will cause complete collapse of the $\Delta\Psi$, maximally increase respiration (in the absence of inhibition), fully release Ca^{2+} ions, and induce maximal swelling in that particular organelle.

Rationale: If the average number of mitochondria isolated from rat liver corresponding to 1 mg of protein is about $9*10^9$ [37], and the V_{maxO2} for uncoupled rat liver mitochondria respiring on succinate is about 350 ng O_2/min/mg of protein [38], then $V_{maxO2}=(350*10^{-9}$ g O_2/min/mg $*$ $6*10^{23})/32$ g (1 mol of O_2 is 32 g, which is equal to $6*10^{23}$ molecules (Avogadro number)), and thus V_{maxO2} is $\sim 10^{16}$ molecules/min/mg of protein. According to the Mitchell chemiosmotic concept, for one O_2 molecule consumed by mitochondria energized by succinate, four electrons will be transferred by the respiratory chain coupled to the transfer of eight protons by the proton pumps to maintain the mitochondrial $\Delta\Psi$. Therefore, V_{maxH+} will be $\sim 8*10^{16}$ protons/min/mg of protein, which is about $1.5*10^5$ H^+/s per single mitochondrion. However, for the active ion channel or open pore (dissipating $\Delta\Psi$), ion flux rate values are $\sim 10^7$ ions/s [39]. Therefore, taking into account the fact that the active proton pump and active ion channel have opposite directions in terms of $\Delta\Psi$, then the opening of even one functional pore per mitochondrion will lead to the complete loss of the $\Delta\Psi$ in that organelle. This reasoning is in agreement with data showing that a single gramicidin channel per chloroplast induces complete collapse of the $\Delta\Psi$ even though the size of this channel is much smaller (conductance of 10 picosiemens [40]) than the mitochondrial pore (a megachannel with a conductance of 1300 picosiemens [41]).

Assumption 2. After pore opening, sucrose influx and subsequent swelling in a single mitochondrion will be much more rapid than the minutes or tens of minutes required to complete pore openings in the total mitochondrial population. Pore opening in a single mitochondrion can therefore be considered mathematically, simply as an immediate event.

Rationale: High rates of ion efflux, and sucrose or water influx are due to high translocation constants through the membrane pores, which may be described by standard equations for passive diffusion from the high to low concentration of solute. Considering that the average number of mitochondria isolated from rat liver is about $9*10^9$ per mg of protein and that a single average mitochondrion has a diameter of about 0.75–1 μm [37,39], one can calculate that mitochondria containing 1 mg of protein occupy a volume of about 10^{-6} liter. Thus, the volume of a single mitochondrion would be approximately 10^{-16} liter. If 10^{-1} M sucrose were to be transported into the mitochondria in the 1-ml cuvette, the diffusion rate would be $6*10^{23}*10^{-1}*10^{-16}=6*10^6$ molecules per second, where $6*10^{23}$ is the Avogadro number.

The open pore has a translocating value of $\sim 10^7$ molecules per second [39]. Thus, the theoretical time for translocation of 10^{-1} M sucrose into 1 mg/ml mitochondria in a 1-ml volume would be about 1–10 s, which is a relatively rapid event, compared to the timeframe of a typical experiment (tens of minutes).

Assumption 3. Similar arguments to those made in the second assumption hold for ions. Specifically, the rates at which ions that have been released from the mitochondria with open pores and have been taken up by the population of mitochondria still having intact membranes are very rapid in comparison to the time of the experiment. Therefore, the rates of ion redistribution can be ignored at this stage of the mathematical modeling.

As a consequence of the above assumptions, the kinetics of the respiration stimulation and dissipation of the $\Delta\Psi$ imply a gradual increase of the portion of mitochondria that have an open pore. In accord with the Massari notation [28], this portion of the mitochondria is designated as a parameter Xp. Massari developed equations based on classic chemical kinetics showing mitochondrial swelling to be reflected by a gradual increase in parameter Xp, which may vary from 0 (when no mitochondria are swollen) to 1 (when all mitochondria are swollen). Since Massari's publication in 1996 [28], there have been no additional reports related to these issues to our knowledge. We have now extended Massari's approach to describe the kinetics of changes in several parameters of mitochondrial functioning. Although the present model is simplified, it can serve as the starting point for further experimental work to obtain insights into the mechanism of the permeability transition.

In our model, we use a simplified treatment of the parameter Xp to test relationships among the four measured parameters. The next four sections link Xp with each measured parameter.

The mitochondrial permeability inducers (Ca^{2+}, PhAsO, and alamethicin) caused a permeability change. As expected, the control with CsA plus Ca^{2+} did not. Therefore, for the control, all the assumptions listed above are not applicable, and the parameter Xp does not exist under such conditions. Thus, this control was excluded from the following analysis.

3.5. Calculation of Xp for swelling

Massari calculated Xp from absorbance changes after MPT induction in mitochondrial suspension by using the following Equation:

$$\mathrm{Xp_{Swell}}(t)=\frac{(\mathrm{A_i}-\mathrm{A})*\mathrm{A_u}}{(\mathrm{A_i}-\mathrm{A_u})*\mathrm{A}} \tag{6}$$

where $\mathrm{Xp_{Swell}}$ is the portion of the mitochondria in the swollen state, A is the absorbance of the mitochondria at a given time, $\mathrm{A_i}$ is the initial absorbance (i.e., for mitochondria under 'State 2' before additions) and $\mathrm{A_u}$ is the absorbance in the completely swollen state (i.e., at the end of the experiment with alamethicin) [28].

3.6. Calculation of Xp for oxygen uptake

Consider a mitochondrial system under specific experimental conditions in which respiration is either coupled (when the electron flow is restricted by only the respiration rate (specific rate is V_{initial})) or uncoupled (specific rate is $V_{\max}$), and Xp is the portion of uncoupled mitochondria (with open pores), then the total respiration rate is:

$$V_{\mathrm{O_2}}=(1-\mathrm{Xp})*M*V_{\mathrm{initial}}+\mathrm{Xp}*M*V_{\max} \tag{7}$$

where M is the mass of mitochondria in the experimental cuvette expressed in mg of protein.

At the beginning of the experiment, when Xp=0, $V_{\mathrm{i}}=V_{\mathrm{initial}}*M$; at the end of the experiment, when Xp=1, $V_{\mathrm{u}}=V_{\max}*M$. A simple transformation gives Eq. (8):

$$\mathrm{Xp_{O_2}}(t)=\frac{(V-V_{\mathrm{i}})}{(V_{\mathrm{u}}-V_{\mathrm{i}})} \tag{8}$$

where V is the rate of oxygen consumption at a given time in $\mu\mathrm{MO_2\ s^{-1}}$.

3.7. Calculation of Xp for $\Delta\Psi$ dissipation

The calculation of $\mathrm{Xp}_{\Delta\Psi}$ is more complicated than the calculation of either $\mathrm{Xp_{Swell}}$ or $\mathrm{Xp_{O2}}$. Consider the following:

1) Under the experimental conditions used, the TPP^+ concentration inside the mitochondria is determined by the potential of the intact (no pore) mitochondria. The balance between the inner and outer TPP^+ concentrations is nonlinear and at room temperature is described as $\frac{[\mathrm{TPP^+}]_{\mathrm{in}}}{[\mathrm{TPP^+}]_{\mathrm{out}}}=10^{\frac{\Delta\Psi}{59}}$ (derived from the Nernst Eq. (1)).
2) The Xp increase and TPP^+ efflux from the portion of the mitochondria that has undergone MPT is accompanied by the rapid reuptake of a portion of the released TPP^+ by mitochondria that still possesses a $\Delta\Psi$ capable of external TPP^+ accumulation. As noted above, we assume that this process is much more rapid compared to the measured overall kinetics of Xp change.

Consider a mass conservation equation for TPP^+ balance in the system at each given period of time. Three pools of TPP^+ exist: $[TPP^+]^{\mathrm{i}}$ for intact mitochondria, $[TPP^+]^{\mathrm{s}}$ for swollen mitochondria, and free TPP^+ in the cuvette. Therefore:

$$\begin{aligned}\mathrm{TPP^{total}}=&[\mathrm{TPP^+}]_{\mathrm{out}}*V'_{\mathrm{out}}\\&+[\mathrm{TPP^+}]^{\mathrm{i}}_{\mathrm{in}}*(1-\mathrm{Xp})*V_{\mathrm{in}}*M\\&+[\mathrm{TPP^+}]^{\mathrm{s}}_{\mathrm{in}}*\mathrm{Xp}*V_{\mathrm{in}}*r*M\end{aligned} \tag{9}$$

where TPP^{total} is the total amount of TPP^+ in the system in μmol; $[TPP^+]_{out}$ is the concentration of free TPP^+ in μM; V'_{out} is the volume of the experimental cuvette in ml; $[TPP^+]^i_{in}$ is the concentration of TPP^+ in the intact mitochondria in μM; $(1-Xp)$ is the portion of intact mitochondria; V_{in} is the specific volume of intact mitochondria in ml/mg; M is the mass of mitochondria in the cuvette in mg of protein; $[TPP^+]^s_{in}$ is the concentration of TPP^+ in the swollen mitochondria in μM; Xp is the portion of the swollen mitochondria; and r is a coefficient for the mitochondrial volume increase due to transition from the intact to the swollen state. The coefficient r can be estimated from the data presented by Beavis and coauthors [29], and for rat liver mitochondria under isotonic conditions, it has a value of less than 2.

According to our first assumption, $[TPP^+]_{out}=[TPP^+]^s_{in}$. Therefore:

$$TPP^{total}=[TPP^+]_{out}*[V_{out}'+Xp*V_{in}*r*M] + [TPP^+]^i_{in}*(1-Xp)*V_{in}*M \quad (10)$$

Since $V'_{out} \gg V_{in}*M$, and also $V'_{out} \gg V_{in}*r*M$ by a factor of ~1000 (when $V'_{out}=1$ ml, $M=1$ mg of protein and osmolarity of the experimental buffer=300 mosM), the coefficient r can be ignored. Therefore Eq. (10) simplifies to Eq. (11):

$$TPP^{total}=[TPP^+]_{out}*V'_{out} + [TPP^+]^i_{in}*(1-Xp)*V_{in}*M \quad (11)$$

This equation shows that all TPP^+ is present either inside the intact mitochondria or in the buffer outside the swollen mitochondria. Under the conditions used in the present experiments, the amount of TPP^+ bound to the discharged mitochondrial membrane in comparison to the TPP^{total} is considered negligible. Therefore, at the zero time of the experiment, when Xp=0:

$$TPP^{total}=I*V'_{out}+[TPP^+]^i_{in}*V_{in}*M \quad (12)$$

where I is the concentration of TPP^+ in μM at the beginning of the experiment when the TPP^+ concentration is stabilized after mitochondrial addition.

At the end point of the experiment, when Xp=1:

$$TPP^{total}=[TPP^+]_{out}*V'_{out}=F*V'_{out} \quad (13)$$

where F is the concentration of TPP^+ in μM after MPT is completely induced in mitochondria.

After algebraic transformations using the equation $\frac{[TPP^+]_{in}}{[TPP^+]_{out}}=10^{\frac{\Delta\Psi}{59}}$, the correlation between Xp and TPP^+ concentration during the experiment becomes:

$$Xp_{\Delta\Psi}(t)=\frac{([TPP^+]-I)*F}{(F-I)*[TPP^+]} \quad (14)$$

where $[TPP^+]$ is the concentration of TPP^+ ions in the buffer at a given time in μM.

3.8. Calculation of Xp for Ca^{2+} release

The parameter Xp_{Ca2+} due to MPT induction in the mitochondria can be estimated in a similar fashion to that calculated for $Xp_{\Delta\Psi}$. The assumptions used for calculating redistribution of the TPP^+ ions between the mitochondria and the buffer during the experimental procedure are also useful for calculating the redistribution of Ca^{2+} ions. Mitochondria possess a highly active Ca^{2+} uniporter [42,43], and thus Ca^{2+} rapidly redistributes as a function of the potential. The equation for the balance between inner and outer Ca^{2+} concentrations is derived from the Nernst Eq. (1) $\frac{[Ca^{2+}]_{in}}{[Ca^{2+}]_{out}}=10^{\frac{\Delta\Psi}{29}}$ and is similar to the equation for the $Xp_{\Delta\Psi}$ (Eq. (14)). Therefore:

$$Xp_{Ca^{2+}}(t)=\frac{([Ca^{2+}]-I)*F}{(F-I)*[Ca^{2+}]} \quad (15)$$

where $[Ca^{2+}]$ is the concentration of Ca^{2+} ions at a given time in μM, the constant F is the $[Ca^{2+}]_{free}$ in μM (the final Ca^{2+} concentration at the end of the experiment was used as the constant F), and constant I is the $[Ca^{2+}]_{initial}$ in μM (i.e., Ca^{2+} concentration in the buffer containing mitochondria in 'State 2' before addition of the agent).

Finally, all four-channel readings can be transformed into the parameter Xp, thus providing a meaningful basis for comparison among all the kinetic parameters recorded from each channel. The corresponding data for all four parameters from Fig. 6 transformed into the dimensionless parameter Xp, which increases from zero with time, are presented in Fig. 8. $T_{1/2}$ values corresponding to the 0.5 Xp value for each kinetic parameter are presented in Table 3. Again, as was noted for the data in Table 2, the $T_{1/2}$ values do not necessarily imply monophasic processes. Differences in $T_{1/2}$ values are convenient indicators of the distinctly different time courses for each of the kinetic parameters. Difference in the kinetics of the changes and $T_{1/2}$ values for all Xp parameters were noted when MPT is induced either by Ca^{2+} or by PhAsO (Fig. 8; Table 3). However, in the case of alamethicin, the $T_{1/2}$ values for Xp_{O2}, Xp_{Ca2+}, and $Xp_{\Delta\Psi}$ did not exhibit significant differences (in agreement with assumptions made above). For all three MPT inducers, the rise in Xp_{Swell} was considerably delayed when compared with the other measured parameters.

Thus, the findings based on the Xp parameters show that the process of MPT induction cannot be simply explained by an increase with time of sequential pore openings in a fraction of the mitochondrial population. This fraction is characterized by complete loss of TPP^+ and Ca^{2+} and has maximal respiration rate and swelling. However, as we discuss below, the above-described approach can be used as

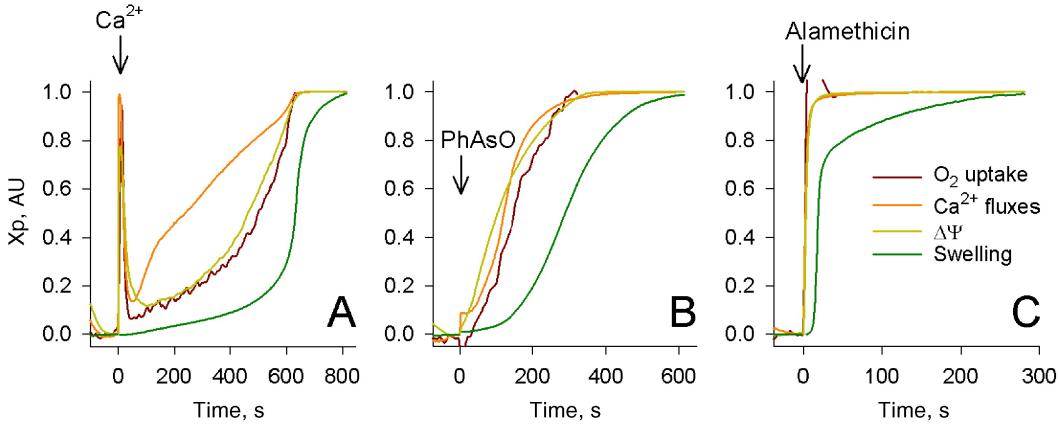

Fig. 8. Superposed and normalized traces of Xp parameters taken from Fig. 6. Shown are the responses of mitochondria due to MPT induction by (A) 100 μM Ca^{2+}, (B) 50 μM PhAsO, and (C) 20 μg/ml alamethicin. Note: all four traces are cut off upon reaching an Xp value of 1 (see the Results section for details and explanation).

a starting point for the multiparameter kinetics analysis of MPT induction.

4. Discussion

4.1. Instrument sensitivity and response

The data presented above clearly demonstrate that the electrodes, sensors and the integrated system are well suited for experiments on isolated mitochondria. The critical instrument characteristics are: 1) high sensitivity and linearity of the individual sensors, 2) ability to operate in a single chamber without 'cross-talk' among the parameters measured, and 3) rapid response times of the system components.

Individual testing of the sensors indicates that all four provide linear signal responses. The regression coefficients within the ranges used in typical mitochondrial experiments were: $r^2_{O2}=0.991$, $r^2_{TPP+}=0.999$, $r^2_{Ca2+}=0.0999$, $r^2_{T660}=0.996$ ($n=6$).

The apparent effect of TPP^+ on the Ca^{2+}-selective electrode response can be attributed to Ca^{2+} contamination in the TPP^+ stock solution, which was determined by independent analysis of the divalent ion content. Ca^{2+} contamination can be eliminated by EGTA chelation of the TPP^+ solution (Fig. 3). In future experiments, it may be important to prepare Ca^{2+}-free TPP^+.

The instrument design utilizes one reference electrode in combination with two ion-selective electrodes. This configuration does not result in any detectable 'cross-talk' between ion-selective electrodes, as illustrated in Fig. 4.

The T_{95} was 1.5±0.1 s for the oxygen electrode, 6.3±0.8 s for the TPP^+-selective electrode and 2.7±0.3 s for the Ca^{2+}-selective electrode. Sequential additions of mitochondria to the chamber suggested that the PD T_{95} was 2.3±0.5 s. Since the response of the PD itself was much faster (<0.1 s), the mixing time must have been on the order of 2 s. The 2 s mixing delay appears to be the major factor limiting response for all the parameters measured, except TPP^+. Therefore, an output-reading interval from 0.1 to 0.5 s is optimal for the sensor's dynamics.

The modular design of the present apparatus allows easy replacement of one or more ion-selective electrodes with electrodes possessing different specifications, thus permitting monitoring parameters of interest (e.g., pH, K^+, Cl^-) other than those measured here.

4.2. Quality control of mitochondrial samples

The very high specific activity of the mitochondrial marker enzyme GDH and the very low specific activity of the cytosolic marker enzyme γ-cystathionase indicated that the mitochondrial fraction was of high purity (see the Experimental section). Contamination of the mitochondria by cytosolic γ-cystathionase was ~0.01%.

The high quality of mitochondrial samples was further confirmed by comparison of the ADP/O ratios and RCR values during the first hour and during 8–12 h after isolation (see Materials and methods). The samples de-

Table 2
$T_{1/2}$ (s) for the measured parameters denoted as a relative change ($n=3$)

Parameter/Inducer	Ca^{2+} 100 μM	PhAsO 50 μM	Alamethicin 20 μg/ml
O_2 uptake	360±77	120±13	1.4±0.6
Ca^{2+} fluxes	570±62	267±22	19.3±1.4
ΔΨ	523±76	280±17	10.0±1.5
Swelling	491±68	235±24	9.9±2.1

Table 3
$T_{1/2}$ (s) for the measured parameters denoted as Xp ($n=3$)

Parameter/Inducer	Ca^{2+} 100 μM	PhAsO 50 μM	Alamethicin 20 μg/ml
O_2 uptake	412±78	140±4	1.5±0.5
Ca^{2+} fluxes	368±85	120±3	6.4±0.5
ΔΨ	195±31	103±3	4.6±0.4
Swelling	553±68	307±29	15.6±3.2

monstrated high constancy in ADP/O ratio and RCR values, exhibiting no significant difference in these parameters during more than 8 h of storage.

4.3. Analysis of mitochondrial experiments

Our analysis is based on the data obtained from the measured mitochondrial parameters and assumption that MPT induction reflects a gradual increase in the portion (Xp) of maximally swollen mitochondria with collapsed $\Delta\Psi$, maximally increased respiration rate and release of Ca^{2+}, as described in the Results section. If this model is correct, the heterogeneity of the mitochondrial population can be functionally represented by the existence of two states, namely $\Delta\Psi$=max and $\Delta\Psi$=0, with a minimal level of transitional (intermediate) states. This assumption is appropriate for some specific applications as described below. The estimated effective size of the mitochondrial pore (which permits the transport of substances up to 1500 Da) is large enough to completely and immediately collapse the $\Delta\Psi$ even if only one pore per single mitochondrion is open. In this respect, as noted above, one gramicidin channel (much smaller than the mitochondrial pore) per single chloroplast completely abolishes its $\Delta\Psi$ [40,41]. Calculations presented in the Results section show that the overall activity of the proton pumps from a single mitochondrion is not sufficient to maintain $\Delta\Psi$ when one pore per mitochondrion is open.

At this point, the question may be reasonably asked: "What is the specific process that is responsible for the differences in the kinetics of Xp (based on the readings from the four parameters measured) when MPT is induced by either Ca^{2+} or PhAsO?" (Fig. 8). The answer to this question may be found in studies where it was suggested that the MPT induction is possibly preceded by the induction of relatively selective ion leaks from the mitochondria [44–48]. As a consequence of the analysis for the parameter Xp presented in the Results section, such ion leaks suggest that some mitochondria are not swollen yet possess low $\Delta\Psi$. The existence of such a mitochondrial sub-population is revealed by the earlier increase in $Xp_{\Delta\Psi}$ compared to the increase in Xp_{Swell}. This might offer an explanation as to why the kinetics of Xp calculated for the four parameters are so different under the specific conditions used. It is clear that in cases where either Ca^{2+} or PhAsO induces the MPT, the Xp_{Swell} exhibits the slowest kinetics compared to other Xp parameters (Fig. 8).

Thus, our kinetic analysis gives us an effective tool for characterization of the process of MPT induction in more details than was previously possible. Apparently, for MPT induction by Ca^{2+} ions (Fig. 8, Panel A), changes in the parameter Xp_{Ca2+} precede those for both Xp_{O2} and $Xp_{\Delta\Psi}$, and more obviously for Xp_{Swell}. This implies that the 'classical non-specific pore induction' is preceded by a relatively selective Ca^{2+} ion leak, followed by mitochondrial uncoupling. The last stage of this process is the development of the non-selective permeability, reflected in the increase of Xp_{Swell}.

In the case of pore induction by PhAsO (Fig. 8, Panel B), the sequence of events is somewhat different. In this case, the change in Xp_{Ca2+} and $Xp_{\Delta\Psi}$ are characterized by similar kinetics, followed sequentially by Xp_{O2} and Xp_{Swell}. The findings can be interpreted as evidence for the induction of a selective electrogenic leak, which causes a fall of the $\Delta\Psi$ and Ca^{2+} release. However, the development of the classical non-selective permeability is delayed in this case.

The above analysis represents a simplified approach, based on the assumption that respiration, Ca^{2+} content, $\Delta\Psi$, and volume changes will exhibit similar kinetics for their Xp parameters. Our finding of deviation from this expected behavior indicates the occurrence of leaks, which result in misalignment of changes in the Xp parameter kinetics.

Our methodology takes the previous approach [28] to the next step because it is based on the real-time simultaneous measurement and comparative kinetic analysis of multiple mitochondrial parameters. The instrumental and computational approaches developed here not only demonstrate the usefulness of the present apparatus, but also show that it is possible to gain insights into the mechanism of MPT induced by different effectors.

Acknowledgements

The authors are grateful to our colleagues: Dr. Lev S. Yaguzhinsky at the A. N. Belozersky Institute of Physico-Chemical Biology of Moscow State University for discussions and advice concerning the design of the apparatus described here; Dr. John P. Blass at the Dementia Research Service of Burke Medical Research Institute; Dr. David G. Nicholls at Buck Institute; and Dr. Alexander Yu. Andreyev for critical reading of the manuscript.

The study was supported in part by grants from Russian Foundation for Basic Research: 98-04-48641 (BFK); 96-04-49384, 02-04-48845 (DBZ) and 00-04-48299, 03-04-48905 (YNA), and from NIH: RO1 NS 38741 (AMB), PO1AG 14390 (BSK) and RO1 ES 08421 (AJLC).

References

[1] D.B. Zorov, B.F. Krasnikov, A.E. Kuzminova, M.Yu. Vysokikh, L.D. Zorova, Mitochondria revisited. Alternative functions of mitochondria, Biosci. Rep. 17 (1997) 507–520.

[2] A.P. Halestrap, G.P. McStay, S.J. Clarke, The permeability transition pore complex: another view, Biochimie 84 (2002) 153–166.

[3] D.R. Hunter, R.A. Haworth, The Ca^{2+}-induced membrane transition in mitochondria: I. The protective mechanisms, Arch. Biochem. Biophys. 195 (1979) 453–459.

[4] R.A. Haworth, D.R. Hunter, The Ca^{2+}-induced membrane transition in mitochondria: II. Nature of the Ca^{2+} trigger site, Arch. Biochem. Biophys. 195 (1979) 460–467.
[5] D.R. Hunter, R.A. Haworth, The Ca^{2+}-induced membrane transition in mitochondria: III. Transitional Ca^{2+} release, Arch. Biochem. Biophys. 195 (1979) 468–477.
[6] M.A. Lessler, Oxygen electrode measurements in biochemical analysis, Methods Biochem. Anal. 17 (1969) 1–29.
[7] E.A. Liberman, V.P. Topaly, L.M. Tsofina, A.A. Jasaitis, V.P. Skulachev, Mechanism of coupling of oxidative phosphorylation and the membrane potential of mitochondria, Nature 222 (1969) 1076–1078.
[8] N. Kamo, M. Muratsugu, R. Hongoh, Y. Kobatake, Membrane potential of mitochondria measured with an electrode sensitive to tetraphenyl phosphonium and relationship between proton electrochemical potential and phosphorylation potential in steady state, J. Membr. Biol. 49 (1979) 105–121.
[9] M.R. Duchen, Mitochondria and calcium: from cell signalling to cell death, J. Physiol. 529 (2000) 57–68.
[10] S. Baudet, L. Hove-Madsen, D.M. Bers, How to make and use calcium-specific mini- and microelectrodes, Methods Cell Biol. 40 (1994) 93–113.
[11] V.A. Tugai, P.V. Usatiuk, Simultaneous recording of Ca^{2+} and pH when studying the processes of calcium transport in sarcoplasmic reticulum, Ukr. Biohim. Z. 51 (1979) 508–510.
[12] E.L. Kholmukhamedov, V.P. Zinchenko, Yu.V. Evtodienko, Self-oscillations of ion fluxes and redox state of the respiratory chain of mitochondria, Biofizika (Russian) XXV 1 (1980) 124–128.
[13] M.C. Beatrice, J.W. Palmer, D.R. Pfeiffer, The relationship between mitochondrial membrane permeability, membrane potential, and the retention of Ca^{2+} by mitochondria, J. Biol. Chem. 255 (1980) 8663–8671.
[14] J. Sanchez Olavarria, C. Galindo, M. Montero, Y. Baquero, J. Victorica, J. Satrustegui, Measurement of 'in situ' mitochondrial membrane potential in Ehrlich ascites tumor cells during aerobic glycolysis, Biochim. Biophys. Acta 935 (1988) 322–332.
[15] B.F. Krasnikov, A.S. Avad, D.B. Zorov, L.S. Yaguzhinsky, Effects of amyl ester of unsubstituted rhodamine on respiration and Ca^{2+} transport in rat liver mitochondria, Biochem. Biophys. Res. Commun. 175 (1991) 1010–1016.
[16] B.F. Krasnikov, A.E. Kuzminova, D.B. Zorov, The Ca^{2+}-induced pore opening in mitochondria energized by succinate–ferricyanide electron transport, FEBS Lett. 419 (1997) 137–140.
[17] F. Ichas, L.S. Jouaville, J.P. Mazat, Mitochondria are excitable organelles capable of generating and conveying electrical and calcium signals, Cell 89 (1997) 1145–1153.
[18] A.E. Kuzminova, A.V. Zhuravlyova, M.Yu. Vyssokikh, L.D. Zorova, B.F. Krasnikov, D.B. Zorov, The permeability transition pore induced under anaerobic conditions in mitochondria energized with ATP, FEBS Lett. 434 (1998) 313–316.
[19] P.X. Petit, M. Goubern, P. Diolez, S.A. Susin, N. Zamzami, G. Kroemer, Disruption of the outer mitochondrial membrane as a result of large amplitude swelling: the impact of irreversible permeability transition, FEBS Lett. 426 (1998) 111–116.
[20] A. Andreyev, G. Fiskum, Calcium induced release of mitochondrial cytochrome *c* by different mechanisms selective for brain versus liver, Cell Death Differ. 6 (1999) 825–832.
[21] Y.E. Kushnareva, M.L. Campo, K.W. Kinnally, P.M. Sokolove, Signal presequences increase mitochondrial permeability and open the multiple conductance channel, Arch. Biochem. Biophys. 366 (1999) 107–115.
[22] L.D. Zorova, B.F. Krasnikov, A.E. Kuzminova, I.A. Polyakova, E.N. Dobrov, D.B. Zorov, Virus-induced permeability transition in mitochondria, FEBS Lett. 466 (2000) 305–309.
[23] N. Brustovetsky, J.M. Dubinsky, Limitations of cyclosporin A inhibition of the permeability transition in CNS mitochondria, J. Neurosci. 20 (2000) 8229–8237.
[24] D. Greiff, C.A. Privitera, Effects of glycerol, freezing and storage at low temperatures, and drying by vacuum sublimation on oxidative phosphorylation by mitochondrial suspensions, Biochim. Biophys. Acta 50 (1961) 233–242.
[25] J. Allsop, R.W. Watts, Methionine adenosyltransferase, cystathionine β-synthase and cystathionine γ-lyase activity of rat liver subcellular particles, human blood cells and mixed white cells from rat bone marrow, Clin. Sci. Mol. Med. Suppl. 48 (1975) 509–513.
[26] B.F. Krasnikov, S.-Y. Kim, S.J. McConoughey, H. Ryu, H. Xu, I. Stavrovskaya, S. Iismaa, B. Mearns, R.R. Ratan, J.P. Blass, G.E. Gibson, A.J.L. Cooper, Transglutaminase activity is present in highly purified non-synaptosomal mouse brain and liver mitochondria, Biochemistry 44 (2005) 7830–7843.
[27] L.C.H. Park, G.E. Gibson, V. Bunik, A.J.L. Cooper, Inhibition of select mitochondrial enzymes in PC12 cells exposed to *S*-(1,1,2,2-tetrafluoroethyl)-L-cysteine, Biochem. Pharmacol. 58 (1999) 1557–1565.
[28] S. Massari, Kinetic analysis of the mitochondrial permeability transition, J. Biol. Chem. 271 (1996) 31942–31948.
[29] A.D. Beavis, R.D. Brannan, K.D. Garlid, Swelling and contraction of the mitochondrial matrix: I. A structural interpretation of the relationship between light scattering and matrix volume, J. Biol. Chem. 260 (1985) 13424–13433.
[30] S.A. Novgorodov, E.V. Kultayeva, L.S. Yaguzhinsky, V.V. Lemeshko, Ion permeability induction by the SH cross-linking reagents in rat liver mitochondria is inhibited by the free radical scavenger, butylhydroxytoluene, J. Bioenerg. Biomembranes 19 (1987) 191–202.
[31] K.M. Broekemeier, M.E. Dempsey, D.R. Pfeiffer, Cyclosporin A is a potent inhibitor of the inner membrane permeability transition in liver mitochondria, J. Biol. Chem. 264 (1989) 7826–7830.
[32] E. Lenartowicz, P. Bernardi, G.F. Azzone, Phenylarsine oxide induces the cyclosporin A-sensitive membrane permeability transition in rat liver mitochondria, J. Bioenerg. Biomembranes 23 (1991) 679–688.
[33] G. Boheim, J.E. Hall, Oscillation phenomena in black lipid membranes induced by a single alamethicin pore, Biochim. Biophys. Acta 389 (1975) 436–443.
[34] V.B. Ritov, I.L. Tverdislova, T.Yu. Avakyan, E.V. Menshikova, Yu.N. Leikin, L.B. Bratkovskaya, R.G. Shimon, Alamethicin-induced pore formation in biological membranes, Gen. Physiol. Biophys. 11 (1992) 49–58.
[35] H. Lecoeur, A. Langonne, L. Baux, D. Rebouillat, P. Rustin, M.C. Prevost, C. Brenner, L. Edelman, E. Jacotot, Real-time flow cytometry analysis of permeability transition in isolated mitochondria, Exp. Cell Res. 294 (2004) 106–117.
[36] B. Chance, G.R. Williams, Respiratory enzymes in oxidative phosphorylation: III. The steady state, J. Biol. Chem. 217 (1955) 409–427.
[37] K. Schwerzmann, L.M. Cruz-Orive, R. Eggman, A. Sanger, E.R. Weibel, Molecular architecture of the inner membrane of mitochondria from rat liver: a combined biochemical and stereological study, J. Cell Biol. 102 (1986) 97–103.
[38] P. Mitchell, J. Moyle, Stoichiometry of proton translocation through the respiratory chain and adenosine triphosphatase systems of rat liver mitochondria, Nature 208 (1965) 147–151.
[39] R.B. Gennis, Biomembranes: Molecular Structure and Function. Springer, Verlag, 1989.
[40] G. Schonknecht, G. Althoff, W. Junge, The electric unit size of thylakoid membranes, FEBS Lett. 277 (1990) 65–68.
[41] P. Bernardi, S. Vassanelli, P. Veronese, R. Colonna, I. Szabo, M. Zoratti, Modulation of the mitochondrial permeability transition pore. Effect of protons and divalent cations, J. Biol. Chem. 267 (1992) 2934–2939.
[42] K.E. Akerman, Changes in membrane potential during calcium ion influx and efflux across the mitochondrial membrane, Biochim. Biophys. Acta 502 (1978) 359–366.

[43] H. Kroner, Ca^{2+} ions, an allosteric activator of calcium uptake in rat liver mitochondria, Arch. Biochem. Biophys. 251 (1986) 525–535.
[44] I. Al-Nasser, M. Crompton, The reversible Ca^{2+} induced permeabilization of rat liver mitochondria, Biochem. J. 239 (1986) 19–29.
[45] M.Kh. Gainutdinov, V.V. Konov, R.N. Ishmukhamedov, T.N. Zakharova, M.A. Khalilova, M.I. Asparov, Oxidative phosphorylation uncoupling in hyperthyroidism as a result of activating cyclosporin-sensitive pores in the inner mitochondrial membrane by water soluble modulators from rat liver cytoplasm, Biochemistry (Moscow) 58 (1993) 629–692.
[46] S.A. Novgorodov, T.I. Gudz, Permeability transition pore of the inner mitochondrial membrane can operate in two open states with different selectivities, J. Bioenerg. Biomembranes 28 (1996) 139–146.
[47] F. Ichas, J.P. Mazat, From calcium signaling to cell death: two conformations for the mitochondrial permeability transition pore. Switching from low- to high-conductance state, Biochim. Biophys. Acta 1366 (1998) 33–50.
[48] M.Y. Balakirev, G. Zimmer, Gradual changes in permeability of inner mitochondrial membrane precede the mitochondrial permeability transition, Arch. Biochem. Biophys. 356 (1998) 46–54.